Journal of Catalysis **181,** 104–112 (1999)
Article ID jcat.1998.2297, available online at http://www.idealibrary.com on IDEAL®

Methane Partial Oxidation by Unsupported and Silica Supported Iron Phosphate Catalysts

Influence of Reaction Conditions and Co-Feeding of Water on Activity and Selectivity

Gokhan O. Alptekin,* Andrew M. Herring,* D. L. Williamson,† Tim R. Ohno,† and Robert L. McCormick*,[1]

*Department of Chemical Engineering and Petroleum Refining, †Department of Physics, Colorado School of Mines, Golden, Colorado 80401-1887

Received June 4, 1998; revised October 6, 1998; accepted October 6, 1998

The partial oxidation of methane to methanol and formaldehyde by molecular oxygen has been investigated over crystalline and silica supported $FePO_4$ at a pressure of 1 atm and in the temperature range of 723–973 K. The quartz phase of $FePO_4$, as well as silica supported $FePO_4$ prepared by impregnation (5 wt%), were examined in a continuous flow reactor. Experiments carried out over $FePO_4$ show high selectivity to formaldehyde at low conversion and suggest that formaldehyde is the primary reaction product, but selectivity decreased rapidly as conversion was increased. The highest space-time yield of formaldehyde observed for this catalyst was 59 g/kg$_{cat}$-h. Above 5% methane conversion, carbon oxides were the only products. For silica-supported $FePO_4$, formaldehyde selectivity did not fall off rapidly, exhibiting a formaldehyde selectivity of 12% at about 10% conversion (STY = 285 g/kg$_{cat}$-h). Quantifiable yields of methanol were observed at very low conversion levels, i.e. below 3% (STY = 11 g/kg$_{cat}$-h). Addition of steam (up to 0.1 atm partial pressure) into the feed stream increased the selectivity to methanol (∼25 g/kg cat/h with up to 3% selectivity) and formaldehyde (∼487 g/kg cat/h with up to 94% selectivity) for the silica-supported $FePO_4$ catalyst. Steam addition had little effect on catalyst activity. Characterization results indicate the presence of $FePO_4$, as well as fivefold coordinate Fe^{3+} in silica supported catalyst samples, and this species is proposed to be responsible for methane activation. After catalysis in the presence of steam, the fivefold coordinate iron is present, but a significant fraction of the $FePO_4$ has been reduced to $Fe_2P_2O_7$. Enhanced selectivity in the presence of steam is attributed in part to the ease of the reversible formation of surface hydroxyl groups (P-OH) from pyrophosphate (P-O-P) groups.

INTRODUCTION

Direct conversion of methane to methanol and formaldehyde in a single catalytic step with sufficiently high yield is a difficult challenge in catalysis. The majority of studies have focused on silica-supported vanadium and molybdenum oxide catalysts (1–3) as silica appears to be the most effective support (4). High selectivity to the desired products is only achieved at low methane conversion. As conversion increases, selectivity to formaldehyde falls off rapidly, as exemplified by the early studies of Spencer with MoO_3/SiO_2 (5) and the more active V_2O_5/SiO_2 (6). Over supported molybdate, methane was converted to formaldehyde and carbon dioxide in parallel reactions. Carbon monoxide was formed by secondary conversion of formaldehyde. Over supported vanadate, a purely sequential reaction path was observed with methane being oxidized to formaldehyde, formaldehyde to CO, and CO to CO_2. The decline in selectivity with increasing conversion can be explained in terms of the relative stability of methane (C-H bond strength 438 kJ mol^{-1}) and formaldehyde (C-H bond strength 364 kJ mol^{-1}). The latter oxidizes readily once formed under typical reaction conditions.

Iron phosphate based catalysts are known to be effective for oxidative dehydrogenation of saturated carboxylic acids to α,β unsaturated acids (7–10). A mixed-valence iron hydroxy phosphate compound is employed industrially in the production of methacrylic acid from isobutyric acid (11, 12). Wang and Otsuka (13, 14) have reported exceptional selectivity for $FePO_4$ in methane and ethane oxidation by O_2, with high yields to partially oxygenated products observed in the presence of H_2, or using N_2O. Additionally, $FePO_4$ exhibits high activity and yield in oxidation of methanol to formaldehyde (15).

Steam effects the crystalline structure of iron phosphate phases leading to formation of mixed valence phosphates and hydroxyphosphates, thought to be the active components of catalysts for oxidative dehydrogenation of isobutyric acid (16, 17). Over Fe-P-O catalysts used industrially, catalytic activity is maintained with time on stream only if a large excess of water vapor was present. Of more relevance for methane partial oxidation, Lunsford has shown that the presence of water is necessary for formation of methanol from surface methoxy groups on both molybdate (18) and

[1] To whom correspondence should be addressed. E-mail: rlmccorm@mines.edu.

0021-9517/99 $30.00

vanadate (19) catalysts. In the present contribution, the effect of reaction conditions, including co-feeding of steam, on methane oxidation activity and selectivity are examined for $FePO_4$ and $FePO_4$ supported on silica.

EXPERIMENTAL

Catalyst Preparation

Bulk $FePO_4$. $FePO_4$ can be prepared in two different structures (20). The first is a quartz-like structure with $P:Fe = 1.0$ containing alternating FeO_4 and PO_4 tetrahedra. A tridymite-type phase is also observed in the presence of excess phosphorous and is stable at lower temperatures (below about 800 K). In this study, the quartz phase of $FePO_4$ was prepared using the method described by Wang and Otsuka (13). Aqueous solutions ($Fe:P = 1$) of $Fe(NO_3)_3$ and $NH_4H_2PO_4$ were mixed and dried at 363 K for 12 h. The precursor obtained was then calcined under flowing air in a tubular furnace at 873 K overnight.

Silica supported $FePO_4$. Silica prepared by precipitation followed by acid washing was used as the support material. The solution of $Fe(NO_3)_3$ and $NH_4H_2PO_4$ described above was used to impregnate the precipitated silica to yield 5% $FePO_4$ by weight. The resulting slurry was dried and activated as described above for bulk $FePO_4$.

Catalyst Characterization

Specific surface areas of the catalyst samples were measured with nitrogen using a Micromeretics 2100E Accusorb Instrument. X-ray powder diffraction (XRD) patterns were obtained using a Rigaku diffractometer with Cu K_α radiation ($\lambda = 1.5432$ Å). Crystal size was estimated from the full width at half maximum of the (102) reflection of $FePO_4$ at $\sim 26^\circ$ two-theta and the Scherrer equation. Transmission infrared spectra were acquired with a BioRad FTS-40 instrument equipped with a DTGS detector. In these *ex-situ* experiments, catalyst samples were mixed with KBr and pressed into pellets. A Kratos Electronics spectrometer with monochromatic Al K_α radiation was used to obtain X-ray photoelectron spectra (XPS). The binding energy of C 1s (284.6 eV) was used as a reference. The surface stoichiometry (P/Fe) was determined using the integrated peak intensities of the Fe $2p_{3/2}$ and P 2p signals, Scofield photoionization cross sections, and the classical relationship given by Scofield (21). Coulston has discussed the difficulties inherent in determining surface stoichiometry for transition metal oxides and phosphates by XPS (22) and shown that for vanadium phosphates, procedures similar to those employed here significantly overestimate the surface phosphorous to metal ratio. This difficulty can be overcome by the use of a suitable set of calibration standards; however, such a calibration has not yet been performed for the iron phosphorous system. Therefore, the absolute values of surface P : Fe reported here are not necessarily meaningful. Comparison of P : Fe values between catalysts in order to examine directional trends should be valid. Mössbauer spectra were recorded at room temperature, using a 25 mCi $^{57}Co/Rh$ source and a conventional constant acceleration spectrometer, operated in triangular mode. Data acquisition was performed with standard multichannel scaling and data analysis was performed by least square fit of Lorentzian lines. By computer folding and fitting, isomer shifts (δ) with respect to α-Fe, quadrupole splittings (Δ) and line widths (Γ) were calculated with a precision about 0.01 mm-s^{-1}. The accuracy for hyperfine field (H) determinations was 0.2 kOe. The samples were diluted in powdered sugar to avoid excessive Mössbauer absorption and pressed into pellets.

Catalyst Testing

Steady-state reactor studies were performed in a fixed bed microreactor in a manner identical to that employed in previous studies (23). The reactor was a quartz tube, 30-cm long and 0.9-cm i.d. at the catalyst bed portion, mounted vertically in a tubular bed furnace. Typically about 0.25 g of bulk $FePO_4$ or 0.1 g of silica-supported $FePO_4$ (screened to 0.2–0.3-mm particle size) was loaded into the reactor and covered with 15-mm layer of quartz beads to obtain a preheating zone and uniform gas distribution. Prior to reaction, the catalyst was calcined *in situ* under helium flow (20 ml/min) at the reaction temperature for one hour. Data was obtained after conditioning the catalyst samples 6 h under reaction conditions. Methane conversion was below 10% for most experiments reported. Carbon balance closures were within ±5% and mostly within ±3%. Fractional conversion and product selectivity were defined as

$$\text{Conversion} = \frac{\text{moles } (CH_3OH + HCHO + CO + CO_2) \text{ formed}}{\text{moles of } CH_4 \text{ fed}},$$

$$\text{Selectivity} = \frac{\text{moles of product formed}}{\text{moles } (CH_3OH + HCHO + CO + CO_2) \text{ formed}}.$$

An on-line Hewlett-Packard 5890 Gas Chromatograph (GC) equipped with a thermal conductivity detector was used to analyze reactant and product streams. The GC system and calibration techniques have been described in detail elsewhere (23).

RESULTS

Reactor Studies

Unsupported $FePO_4$. Figure 1 presents selectivity to HCHO, CO, and CO_2 as a function of CH_4 conversion at $CH_4:O_2$ of roughly 12. Conversion was varied by varying

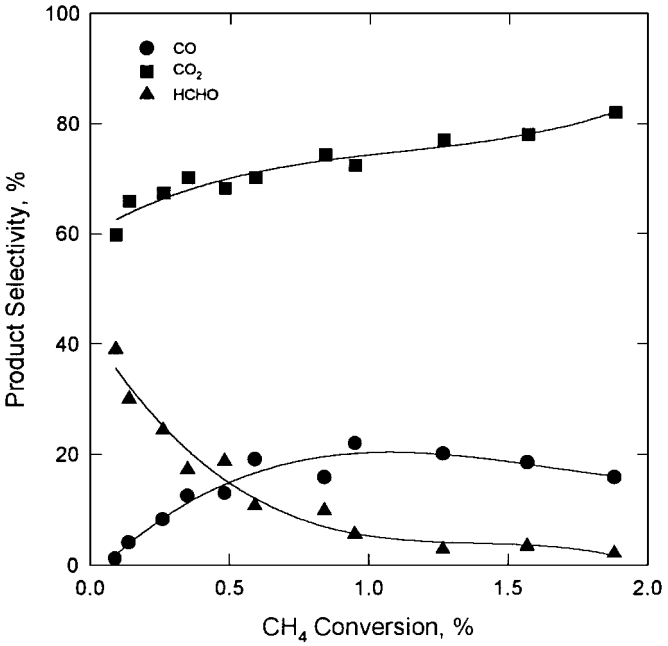

FIG. 1. Product selectivity (%) as a function of methane conversion (%) for unsupported $FePO_4$. GHSV = 10,000–30,000 h^{-1}, $P_{CH4} = 37.6$ kPa, $P_{O2} = 3.1$ kPa, balance He, $T = 848$, and 898 K.

temperature and gas hourly space velocity (GHSV). Selectivity to HCHO was about 40% for methane conversions approaching zero, suggesting that it is a primary reaction product. Selectivity falls rapidly as methane conversion increases, and it drops below 5% at about 2% methane conversion. A consequent increase in selectivity to CO indicates that HCHO is sequentially converted to CO. CO and CO_2 were the only products observed above 5% methane conversion. CO selectivity approaches zero at very low conversion, which confirms that it is a secondary reaction product. Note that even at low conversion a high selectivity to CO_2 is observed (about 60% at zero conversion). This indicates the presence of a direct oxidation path from CH_4 to CO_2, as shown in the following network (oxygen and water molecules not shown), which is similar to that proposed for silica supported molybdate by Spencer (5):

$$CH_4 \rightarrow HCHO \rightarrow CO, \quad [1]$$

$$CH_4 \rightarrow CO_2. \quad [2]$$

A few experiments were conducted at a $CH_4 : O_2$ of 2, where selectivity to CO_2 was much lower at low conversion but was still greater than zero. Apparently the relative rates of the parallel reaction paths are dependent upon the methane to oxygen ratio and suggest that the methane conversion rate is not zero order in oxygen partial pressure. This is in contrast to the zero-order dependence observed over silica-supported molybdate and vanadate catalysts (5, 6).

The effect of CH_4 and O_2 partial pressure was examined to determine parameters for a power-law rate model. Methane partial pressure was varied in the range of 16.7 to 82.2 kPa keeping oxygen partial pressure constant at 3.1 kPa. Similarly, oxygen partial pressure was varied in the 6.2–49.8 kPa range for a constant methane partial pressure of 49.8 kPa. Reaction orders for methane and oxygen were estimated to be 0.66 ± 0.07 and 0.45 ± 0.05, respectively. Kinetic parameters are summarized in Table 1. These experiments were repeated at different temperatures, and the influence of temperature on reaction order was found negligible in the 773–923 K range. The activation energy for methane conversion was estimated as 164 ± 9 kJ/mol.

Silica-supported $FePO_4$. Supporting $FePO_4$ on silica caused an appreciable improvement in per unit surface area catalytic activity and on selectivity. High selectivity to formaldehyde was observed along with quantifiable amounts of methanol. Figure 2 presents the product selectivity as a function of methane conversion at two methane-oxygen ratios. Activity and selectivity were constant over the 72-h duration of the experiments. Relatively high

TABLE 1

Kinetic Parameters and Yields for CH_4 Oxidation over Bulk and Silica-Supported $FePO_4$

Catalyst	Reaction order			Activation energy, kJ/mole	Preexponential factor, mole/m^2-kPa^n-h	Maximum STY, g/kg_{cat}-h		Conversion rate, mole/m^2-h at 873 K
	CH_4	O_2	H_2O			HCHO	CH_3OH	
$FePO_4$	0.66 ± 0.07	0.45 ± 0.05	—	164 ± 9	10,300	59[a]	0	1.2×10^{-4}
$FePO_4$/SiO_2	0.61 ± 0.07	0.28 ± 0.03	—	144 ± 4	2465	285[b]	11	1.9×10^{-4}
	0.48 ± 0.05	0.21 ± 0.03	0.23 ± 0.04	155 ± 3	16,920	487[c]	25	1.7×10^{-4}

Note. Arrhenius parameters obtained at $CH_4 : O_2 = 2$.

[a] $T = 873$ K, GHSV = 30,000 h^{-1}, $P_{CH4} = 37$ kPa, $P_{O2} = 6$ kPa, $W_{cat} = 0.25$ g.

[b] $T = 873$ K, GHSV = 60,000 h^{-1}, $P_{CH4} = 49$ kPa, $P_{O2} = 49$ kPa, $W_{cat} = 0.1$ g.

[c] $T = 873$ K, GHSV = 60,000 h^{-1}, $P_{CH4} = 49$ kPa, $P_{O2} = 49$ kPa, $W_{cat} = 0.1$ g.

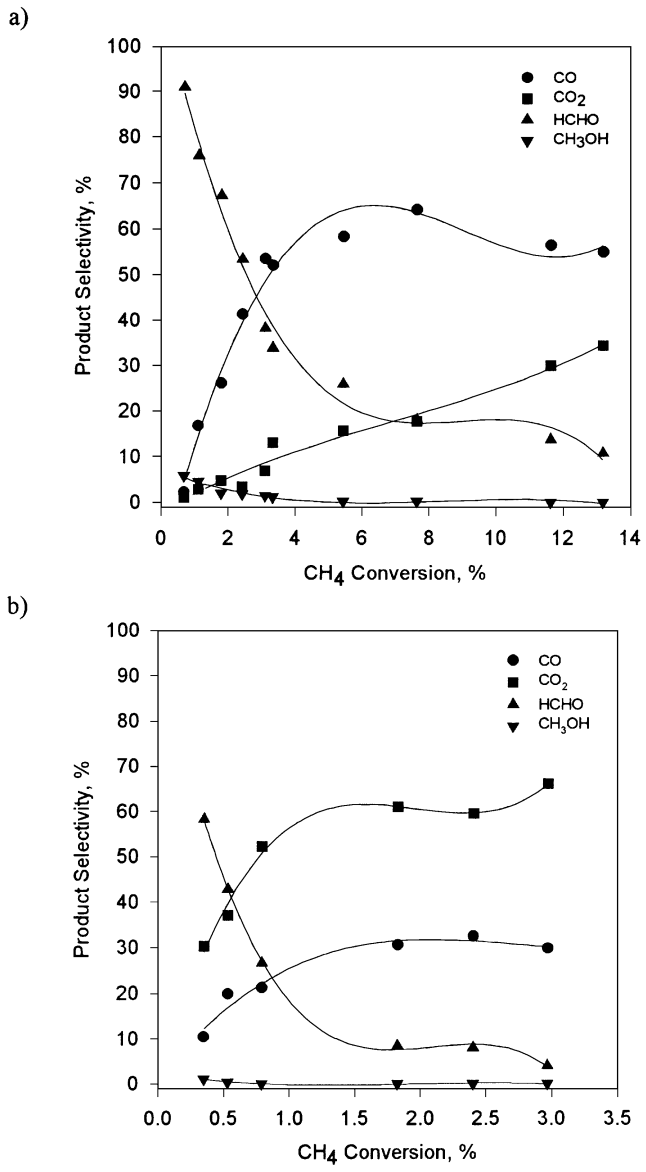

FIG. 2. Product selectivity (%) as a function of methane conversion (%) for $FePO_4/SiO_2$ catalyst (2 wt% Fe). (a) $P_{CH4} = 32.9$ kPa, $P_{O2} = 32.9$ kPa, balance He, $T = 873$–923 K, GHSV = 10,000–60,000 h^{-1}. (b) $P_{CH4} = 59.1$ kPa, $P_{O2} = 5.9$ kPa, balance He, $T = 873$–898 K, GHSV = 22,000–38,000 h^{-1}.

(>10%) formaldehyde selectivity is observed at above 10% methane conversion, even at a methane-to-oxygen ratio of 1 (Fig. 2a). Low but quantifiable selectivity to methanol is observed below 3% conversion under these conditions. At the lowest conversion level of 0.7%, methanol selectivity was 5.8%. The selectivity/conversion pattern suggests a sequential reaction network, similar to that proposed for silica supported vanadate by Spencer (6):

$$CH_4 \rightarrow CH_3OH \rightarrow HCHO \rightarrow CO \rightarrow CO_2. \qquad [3]$$

However, the possibility that methanol and formaldehyde are formed in separate, parallel paths cannot be ruled out based on the present data.

At a methane-to-oxygen ratio of 10 (Fig. 2b) formaldehyde selectivity has decreased to 4% at only 3% conversion (compared to 38% selectivity at methane-to-oxygen ratio of 1; Fig. 2a). Only trace levels of methanol are observed at any conversion level, and the selectivity conversion pattern indicates that CO and CO_2 are secondary reaction products under these conditions. However, selectivity to CO_2 is now much higher than selectivity to CO, the opposite of what was observed at lower $CH_4 : O_2$ ratio. At higher methane : oxygen ratio the catalyst may become over reduced so that partially oxidized intermediates are more strongly bound and therefore more rapidly converted to CO_2.

Reaction orders in methane and oxygen over silica supported $FePO_4$ were determined through a similar set of experiments as described for the unsupported catalyst. Reaction orders were calculated to be 0.61 ± 0.07 and 0.28 ± 0.03, respectively, for methane and oxygen (Table 1). Within experimental uncertainty, reaction order in methane is unchanged relative to bulk $FePO_4$, but it is significantly lower for oxygen. This may indicate that catalyst reoxidation or oxygen adsorption is more rapid for the supported catalyst. The activation energy was found to be 144 ± 4 kJ/mole.

Effect of steam addition. Steam partial pressure was varied in the range of 3.1 to 9.0 kPa over supported and crystalline $FePO_4$. For unsupported $FePO_4$, addition of steam has little effect on activity or on formaldehyde selectivity. For silica-supported $FePO_4$, steam partial pressure has a noticeable influence on the selectivity of the catalyst, while the activity is only slightly effected. As the conversion-selectivity pattern presented by Fig. 3 indicates, the addition of steam increases formaldehyde and decreases CO_2 selectivity. In Fig. 4, space-time-yields (STY) to the desired products are compared in the absence and presence of water as a function of gas hourly space velocity. Addition of steam causes a positive effect on yield, increasing STY of formaldehyde to 487 g/kg_{cat}-h and of methanol to 25 g/kg_{cat}-h.

The effect of steam on reaction order was also investigated by varying steam partial pressure in the range 3.1 to 9.0 kPa at constant methane to oxygen ratio and by varying methane and oxygen partial pressure as described above, but at a steam partial pressure of 3.1 kPa. Reaction orders were found to be 0.48 ± 0.05 for methane, 0.21 ± 0.03 for oxygen, and 0.23 ± 0.04 for water (Table 1). The activation energy in the presence of steam was 134 ± 4 kJ/mole.

Catalyst Characterization

Surface area. Surface areas of 8.6 ± 0.2, 141 ± 3, 81 ± 2 m^2/g were found for bulk $FePO_4$, the silica support, and silica-supported $FePO_4$, respectively. Surface areas of $FePO_4$ catalysts reported in the literature range from 1.8

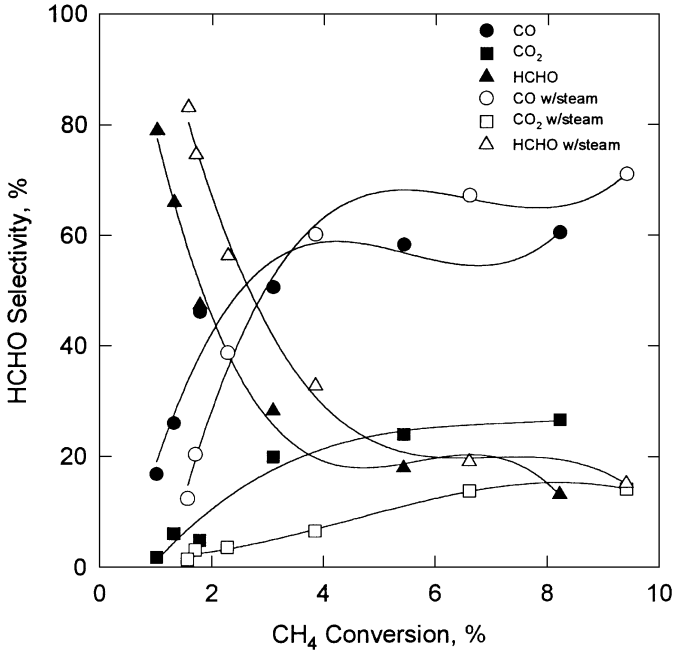

FIG. 3. Effect of steam addition on selectivity pattern for silica supported $FePO_4$. GHSV = 10,000–60,000 h^{-1}, $P_{CH4} = 32.9$ kPa, $P_{O2} = 32.9$ kPa, balance He, $T = 873$ K.

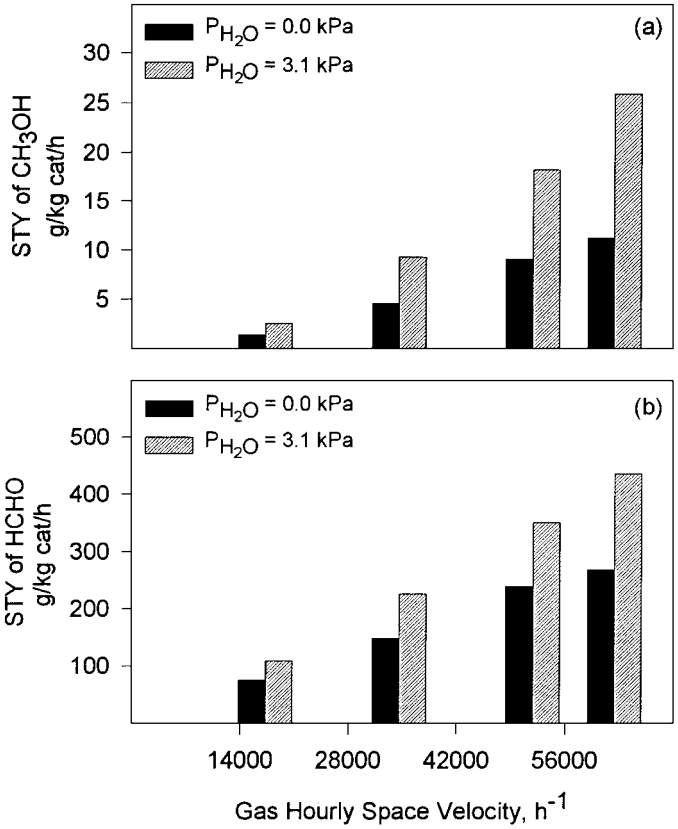

FIG. 4. Effect of steam addition on space-time yield of HCHO and CH_3OH over silica supported $FePO_4$ catalyst. $P_{CH4} = 32.9$ kPa, $P_{O2} = 32.9$ kPa, balance He, $T = 873$ K.

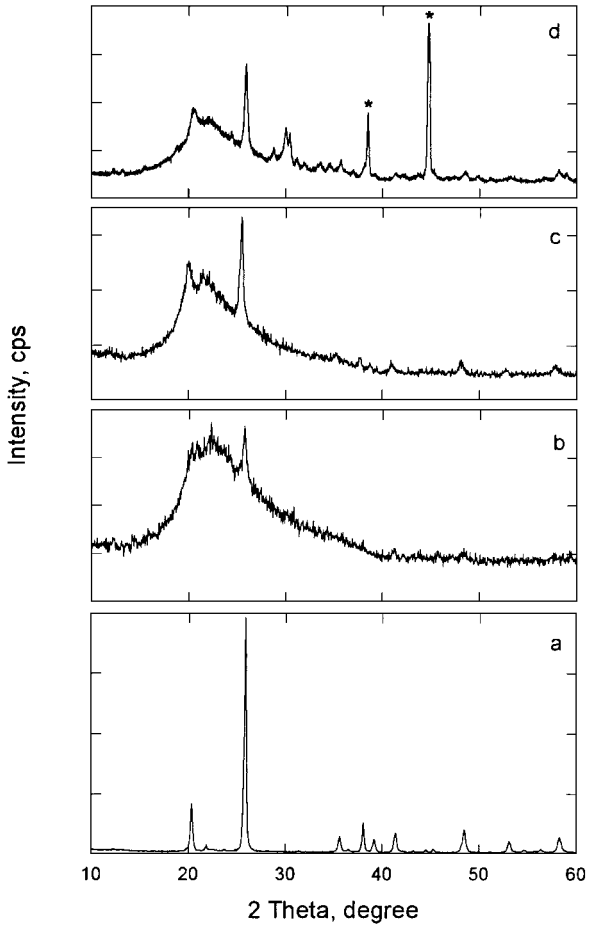

FIG. 5. XRD pattern of the (a) unsupported $FePO_4$, (b) fresh, (c) 48-h aged, (d) 48-h steam-aged silica-supported $FePO_4$ catalyst ($*$ = peaks of aluminum sample holder).

to 15 m^2/g (12, 13, 24). The supported $FePO_4$ catalyst has a significantly lower surface area than the support material, which might be explained by pore blockage by $FePO_4$ crystals.

XRD. The X-ray diffraction pattern for bulk $FePO_4$ is reported in Fig. 5. The only peaks observed correspond to the quartz phase of this material (11), the most intense at 25.8 and 20.1° 2θ. No significant change in relative intensities, or new reflections, was observed after use in methane oxidation in the presence or absence of steam. XRD patterns of fresh and aged silica supported $FePO_4$ are also presented in Fig. 5. The pattern of the fresh catalyst exhibits a sharp peak at 25.8 and a weaker peak at 20.1° 2θ, over a broad background characteristic of amorphous silica, indicating that quartz $FePO_4$ was successfully prepared on the support. Upon exposure to reaction conditions (no steam) for 48 h, the peaks of $FePO_4$ are more intense and many minor peaks of this phase are now evident. Estimation of the mean crystal size from the XRD peak width indicates crystals with a mean diameter of 235 Å for both fresh and

aged catalysts. The enhanced resolution of this component in the aged catalyst XRD pattern must therefore indicate formation of additional $FePO_4$ crystals from an X-ray amorphous phase under reaction conditions. Mössbauer results described below confirm that roughly half of the iron is present in an X-ray amorphous phase. Note that the fresh catalyst was activated at 873 K for 16 h but methane oxidation experiments were conducted at temperatures up to 973 K. Both the longer time at elevated temperature and the higher temperature might account for this increase in crystalline $FePO_4$ content.

The peaks of $FePO_4$ are present in the XRD pattern of the steam-aged catalyst. However, two additional peaks at 29.5 and 31.0° 2θ are also observed. These peaks correspond to the most intense reflections of $Fe_2P_2O_7$ (11) and several minor peaks of this phase are present. The presence of weak peaks at roughly 19, 21, 25, 35, and 36° 2θ is consistent with the presence of $Fe_3(P_2O_7)_2$ (25) but not conclusive, given the low intensity, peak broadness, and complexity of the powder pattern. A peak at 28.8° 2θ and could not be conclusively assigned.

FTIR. The transmission IR spectrum of crystalline $FePO_4$ is shown in Fig. 6. Bands attributed to the various stretching (1000–1200 cm^{-1}) and bending (400–700 cm^{-1}) modes of PO_3-groups are evident (11, 26, 27). No new bands are observed after use in the presence of steam. For supported $FePO_4$, as also shown in Fig. 6, the $\nu(PO_3)$ envelope is narrower and there is only a single strong $\delta(PO_3)$ band at 475 cm^{-1}. After use in the presence of steam, the formation of a distinct band at 802 cm^{-1} is observed. Bands in the 740 and 930 cm^{-1} range are assigned to symmetrical and asymmetrical vibrations of P-O-P groups (11, 26, 27). P-O-P groups are not present in $FePO_4$, which consists of alternating Fe-O and P-O tetrahedra. The observation of the 802 cm^{-1} IR band is thus consistent with formation of pyrophosphate groups.

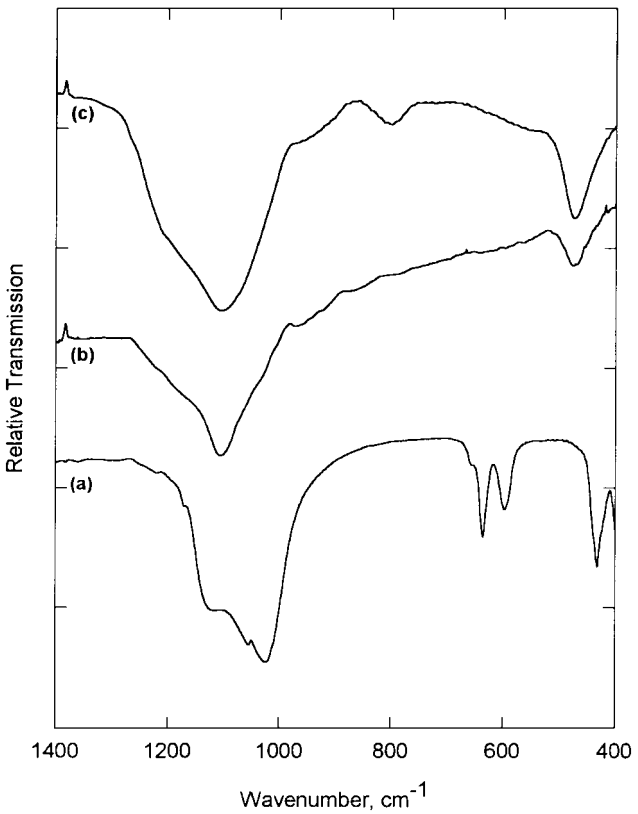

FIG. 6. Transmission IR spectra of the (a) unsupported $FePO_4$, (b) fresh, and (c) 48-h steam-aged silica-supported $FePO_4$ catalyst.

TABLE 2

XPS Binding Energies and Surface Atomic Ratios for Crystalline and Supported $FePO_4$ Catalysts before and after Catalysis (Reference to C 1s at 284.6 eV)

Catalyst	Fe $2p_{3/2}$ (eV)[a]	P 2p (eV)	P/Fe Ratio
$FePO_4$, fresh	712.5 (3.7)[b]	133.5 (1.9)	0.92
$FePO_4$, steam-aged	711.8 (3.9)	133.5 (2.1)	1.10
$FePO_4/SiO_2$, fresh	711.9 (4.7)	133.3 (2.1)	1.07
$FePO_4/SiO_2$, aged	712.3 (4.4)	133.9 (2.0)	1.10
$FePO_4/SiO_2$, steam-aged	711.0 (4.5)	133.8 (2.2)	1.10

[a] Binding energies are reliable within ±0.3 eV.

[b] The values in parenthesis indicate full width at half maximum (FWHM).

XPS. The XPS binding energies (BE) and the surface P/Fe atomic ratios for the crystalline and supported $FePO_4$ catalysts before and after catalytic reaction are given in Table 2. For crystalline $FePO_4$, a Fe $2p_{3/2}$ BE of 712.5 eV with full width at half-maximum (FWHM) of 3.7 eV is observed. Wang and Otsuka report the Fe $2p_{3/2}$ BE in this compound to be 713.2 eV. There is a shift of 0.7 eV to a lower BE after use in the presence of steam. The P 2p peak position remained unchanged at 133.5 eV. Exposure to steam under reaction conditions caused a small increase in the surface P/Fe ratio.

For silica supported iron phosphate, Fe $2p_{3/2}$ was initially observed at 711.9 eV (FWHM = 4.7) and P/Fe was 1.07. Interaction with the silica support causes a shift to lower BE, broadening of the signal, and surface enrichment in phosphorous relative to unsupported $FePO_4$. Upon exposure to reaction conditions with out steam, there is a small increase in the Fe $2p_{3/2}$ BE. A 0.9 eV shift to lower BE is observed with use in the presence of steam, accompanied by a 0.6 eV change in the P 2p peak energy. The surface P/Fe ratio remained unchanged. Using XPS for identification and quantification of the Fe oxidation state is sometimes inaccurate due to the small separation between Fe^{3+} and Fe^{2+}, and the presence of extensive matrix-dependent loss features that severely distort the true spectral background (28). However, Hawn and DeKoven (29) reported a 0.9 eV binding energy difference between FeO and α-Fe_2O_3 (709.7

and 710.6 eV, respectively). Highly electronegative phosphorous in the iron environment causes the binding energy to be observed at higher values for phosphates. Bonnet and coworkers (26) report a separation of 1.9 eV between the BE of the Fe^{3+} and Fe^{2+} oxidation states (710 and 711.9 eV, respectively) for $Fe_2P_2O_7$ that had been exposed to catalytic oxidation conditions. The 0.9 eV shift observed here is thus large enough to be attributed to partial reduction of Fe on the surface of the steam-aged sample. It was not possible to deconvolute the XPS spectrum and quantify the relative amounts of Fe^{2+} and Fe^{3+} because the weakness of the Fe $2p_{3/2}$ signal as a result of the low loading level in the supported catalyst.

Mössbauer spectroscopy. A Mössbauer spectrum of bulk $FePO_4$ after synthesis is presented in Fig. 7 and the related hyperfine interaction parameters are listed in Table 3. The spectrum of the compound as prepared is very similar to that reported in the literature (30). The spectrum can be fit with a Fe^{3+} doublet exhibiting hyperfine interaction parameters characteristic of ferric iron tetrahedrally coordinated by oxygen. A second Fe^{3+} component is also present in very small quantities and suggests that some impurity phase is present at low concentration. After catalysis, in the presence or absence of steam, hyperfine interaction parameters for the dominant component do not change significantly and no new components appear in the spectrum. The amount of impurity phase present decreased after use.

Mössbauer spectra and hyperfine interaction parameters for silica-supported $FePO_4$, after synthesis and exposure to catalytic reaction conditions, are also presented in Fig. 7 and Table 3. For the fresh catalyst, two forms of Fe^{3+} are evident with comparable abundance. The two different forms

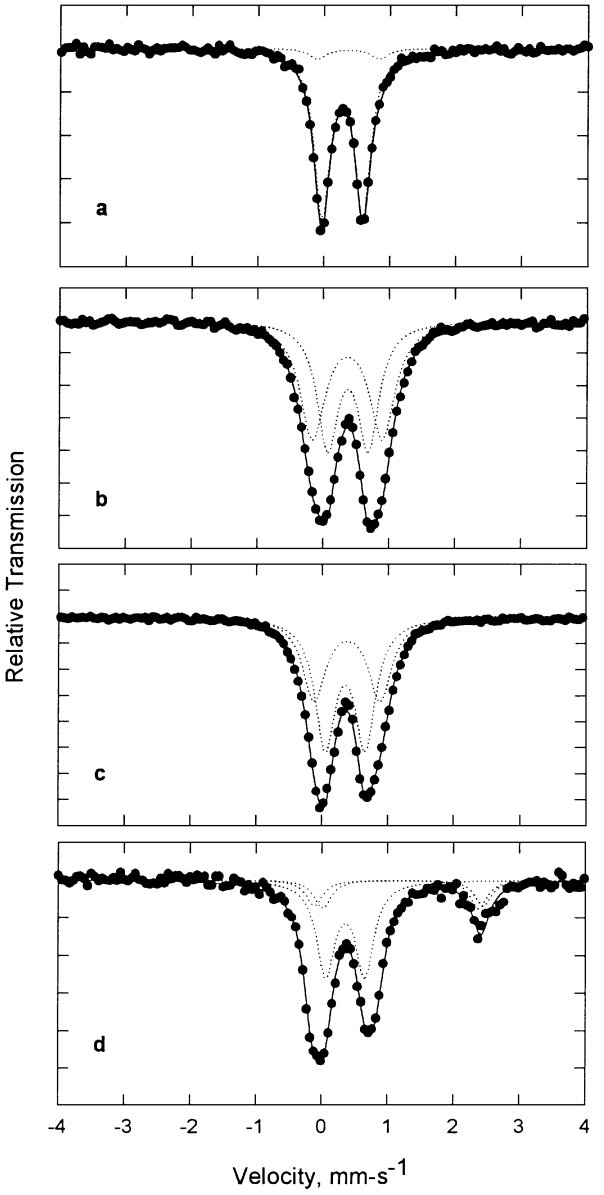

FIG. 7. Mössbauer spectra of the (a) unsupported $FePO_4$, (b) fresh, (c) 48-h aged, (c) 48-h steam-aged silica-supported $FePO_4$ catalysts.

TABLE 3

Hyperfine Interaction Parameters Computed from the Spectra of Unsupported and Silica-Supported $FePO_4$

Catalyst	Component		δ^a (mm/s)	Δ^b (mm/s)	Γ^c (mm/s)	F (%)
Unsupported	(1)	Fe^{3+}	0.282 (5)[d]	0.62 (1)	0.29 (1)	93
	(2)	Fe^{3+}	0.300 (1)	0.90 (1)	0.30 (1)	7
Fresh supported	(1)	Fe^{3+}	0.380 (4)	0.61 (2)	0.38 (1)	47
	(2)	Fe^{3+}	0.372 (4)	1.06 (3)	0.46 (1)	53
Aged supported	(1)	Fe^{3+}	0.354 (2)	0.61 (1)	0.37 (1)	57
	(2)	Fe^{3+}	0.381 (3)	1.00 (3)	0.42 (1)	43
Steam-aged	(1)	Fe^{3+}	0.39 (1)	0.59 (6)	0.33 (4)	41
	(2)	Fe^{3+}	0.37 (1)	0.98 (4)	0.32 (5)	37
	(3)	Fe^{2+}	1.23 (f)[e]	2.37 (f)	0.11 (3)	11
	(4)	Fe^{2+}	1.20 (f)	2.56 (f)	0.10 (3)	11

[a] Isomer shift.
[b] Quadrupolar splitting.
[c] Line width.
[d] The values in parenthesis represents the experimental uncertainty.
[e] Fixed parameter.

were also observed for the catalyst used in methane oxidation in the absence of water. Component 1 is very similar to crystalline $FePO_4$; however, the isomer shift is significantly higher. Component 2 has similar hyperfine interaction parameters to iron in trigonal bipyramid coordination (31) and suggests that interaction with the support increases the number of oxygen atoms in the iron coordination sphere for a fraction of the supported phase. The spectrum after catalytic reaction in the presence of water exhibited three peaks, which can be fit to two ferric and two ferrous components. The ferric components are essentially identical to those observed in the fresh silica supported sample. The best fit of the data was obtained by assigning the interaction

parameters reported for $Fe_2P_2O_7$ (30) to the two ferrous components.

DISCUSSION

Unsupported $FePO_4$ exhibited significant selectivity to formaldehyde in methane partial oxidation. The maximum space time yield observed was 59 g/kg$_{cat}$-h. We estimate a space time yield to formaldehyde of 5 g/kg$_{cat}$-h from data reported by Wang and Otsuka (13) for methane oxidation over $FePO_4$ at 673 K, GHSV $\sim$ 7500, and a methane : oxygen ratio of 4. The higher yield obtained in the present study is most likely because of more optimal reaction conditions (higher space velocity and temperature). The methane conversion rate at 873 K over $FePO_4$ was 1.2×10^{-4} mol/m^2-h (Table 1). This is significantly higher than the rate over V_2O_5/SiO_2 under similar conditions that we calculate to be 4.1×10^{-5} mol/m^2-h from the kinetic parameters of Spencer (6).

Silica-supported iron phosphate exhibited dramatically higher yield of formaldehyde, and a significant yield of methanol. Maximum space-time yields for formaldehyde and methanol were 285 and 11 g/kg$_{cat}$-h, respectively. Methane conversion rate at 873 K was also higher than for unsupported $FePO_4$ (Table 1), and likewise higher than reported for V_2O_5/SiO_2 (6). XRD indicates the presence of crystalline $FePO_4$ in the silica supported catalyst, and this is confirmed by Mossbauer spectroscopy. However, the isomer shift is slightly higher than for bulk $FePO_4$, suggesting a higher electron density on the iron atom. Mossbauer spectra also indicate that roughly one half of the iron is in a very different chemical environment than the tetrahedral coordination of $FePO_4$. The quadropole splitting of this component is typical of five-coordinate Fe, as reported for ferric oxyphosphate, $Fe_3(PO_4)O_3$, by De Guire and coworkers (31). XRD studies (32) have shown that Fe in ferric oxyphosphate occupies the center of a trigonal bipyramid of oxygen atoms. Interaction of $FePO_4$ with SiO_2 apparently produces Fe in a similar coordination. Studies where the loading of $FePO_4$ on SiO_2 was varied from 2 to 16 wt% indicate that the fraction of fivefold coordinated iron decreases with increasing loading. The yield of oxygenated products also correlated with the amount of the five-coordinate phase (33). This structure may be easily reducible and provide highly reactive oxygen species for methane activation. The reduced iron site/oxygen vacancy left behind after a methane oxidation event must also be easily reoxidized to complete the catalytic cycle, consistent with the lower reaction order in oxygen partial pressure as compared to unsupported $FePO_4$.

Silica-supported iron phosphate exhibited maximum space-time yield for formaldehyde and methanol of 487 and 25 g/kg$_{cat}$-h, respectively, in the presence of steam, substantially higher than under dry conditions. This increase in yield was caused by increases in methanol and formaldehyde selectivity, but not in the methane oxidation rate. Steam is known to effect the catalytic activity and selectivity of iron phosphate catalysts used in oxidative dehyrogenation of isobutyric acid by promoting a change in catalyst structure to form hydroxy phosphates (7). No evidence for the formation of these compounds was observed in the present study; however, much higher steam partial pressures are used in the industrial process than employed here.

Mössbauer and infrared spectroscopy, and XRD results, indicate partial transformation of the supported iron phosphate into ferrous pyrophosphate, $Fe_2P_2O_7$. Muneyama and co-workers have also demonstrated that $FePO_4$ can be reduced to $Fe_2P_2O_7$ under catalytic oxidation conditions (11). Iron in ferrous pyrophosphate is octahedrally coordinated by oxygen. Wang and Otsuka (13) found ferrous pyrophosphate itself to be less active for methane oxidation than $FePO_4$, suggesting that methane activation is not enhanced by having Fe^{2+} in this coordination environment. However, P-O-P bridges, characteristic of pyrophosphate and shown to be present by FTIR, may easily and reversibly form surface hydroxyl groups by reaction with water:

$$\text{P-O-P} + H_2O \leftrightarrow 2\,\text{P-OH}. \qquad [4]$$

Improved selectivity may be related to the ease of water desorption, as well as the ease of hydroxyl group formation upon dissociative methane adsorption to form hydroxyl and methoxy. It is notable that Lunsford and coworkers (18, 19) and Khan and Somorjai (34) reported that water vapor plays an essential role in the production of methanol over MoO_3- and V_2O_5-based catalysts. A high concentration of surface hydroxyl groups may favor desorption of the methoxy intermediate as methanol. The presence of pyrophosphate and enrichment of the surface in phosphorus as shown by XPS suggest that the surface of silica-supported $FePO_4$ has a high concentration of sites that can form surface hydroxyl.

A large fraction of the iron remains in the fivefold coordinate phase in the presence of steam. Suggestively, the unassigned X-ray reflection at 28.8° 2θ corresponds to the most intense reflection of the reference phase that we have used for this coordination, ferric oxyphosphate (32). As noted above, this site is proposed to be responsible for methane activation by providing highly reactive lattice oxygen or a site for chemisorption of reactive oxygen species. Methane oxidation rate was essentially unaffected by the presence of steam, suggesting that the sites responsible for methane activation are not altered. Reaction orders in methane and oxygen are also not changed in the presence of steam, within the experimental uncertainty, consistent with this conclusion. A positive reaction order in steam partial pressure suggests participation of surface hydroxyl groups in the reaction. The presence of a high concentration of surface hydroxyls near the methane activation site is likely responsible for improved selectivity under these conditions.

ACKNOWLEDGMENTS

The financial support for this work by the U.S. Department of Energy, Fossil Energy Branch under Contract DE-AC22-PC92110 is gratefully acknowledged.

REFERENCES

1. Hall, T. J., Hargreaves, J. S. J., Hutchings, J. D., Joyner, R. W., and Taylor, S. H., *Fuel Proc. Technol.* **42**, 151 (1995).
2. Parkyns, N. D., Warburton, C. I., and Wilson, J. D., *Catal. Today* **18**, 385 (1993).
3. Brown, M. J., and Parkyns, N. D., *Catal. Today* **8**, 305 (1991).
4. Parmaliana, A., Frusteri, F., Miceli, D., Mezzapica, A., Scurrell, M. S., and Giordano, N., *App. Catal.* **78**, L7 (1991).
5. Spencer, N. D., *J. Catal.* **109**, 187 (1988).
6. Spencer, N. D., and Pereira, C. J., *J. Catal.* **116**, 399 (1989).
7. Muneyama, E., Kunishige, A., Ohdan, K., and Ai, M., *Appl. Catal. A: General* **116**, 165 (1994).
8. Millet, J. M. M., Vedrine, J. C., and Hequet, G., *Stud. Surf. Sci. Catal.* **55**, 833 (1990).
9. Millet, J. M. M., Rouzies, D., and Vedrine, J. C., *Appl. Catal. A: General* **124**, 205 (1995).
10. Vedrine, J. C., Millet, J. M. M., and Volta, J. C., *Catal. Today* **92**, 115 (1996).
11. Muneyama, E., Kunishige, A., Ohdan, K., and Ai, M., *J. Catal.* **158**, 378 (1996).
12. Bonnet, P., and Millet, J. M. M., *J. Catal.* **161**, 198 (1996).
13. Wang, Y., and Otsuka, K., *J. Catal.* **155**, 256 (1995).
14. Wang, Y., and Otsuka, K., *J. Catal.* **171**, 106 (1997).
15. Klissurski, D., Rives, V., Abadzhjieva, N., Pesheva, Y., Pomonis, P., Sdovkos, T., and Petrakis, D., *Chem. Commun.*, 1606 (1993).
16. Virely, C., Forrisier, M., Millet, J. M. M., and Vedrine, J. C., *J. Mol. Catal.* **71**, 199 (1992).
17. Rouzies, D., Millet, J. M. M., Siew, H. S. D., and Vedrine, J. C., *Appl. Catal. A: Gen.* **124**, 189 (1995).
18. Liu, R. S., Liew, K. Y., Johnson, R. E., and Lunsford, J. H., *J. Am. Chem. Soc.* **106**, 4117 (1984).
19. Pak, S., Smith, C. E., Rosynek, M. P., and Lunsford, J. H., *J. Catal.* **165**, 73 (1997).
20. Millet, J. M. M., and Vedrine, J. C., *Appl. Catal.* **76**, 209 (1991).
21. Scofield, J. H., *J. Electron Spectr. Relat. Phenom.* **8**, 129 (1976).
22. Coulston, G. W., Thompson, E. A., and Herron, N., *J. Catal.* **163**, 122 (1996).
23. McCormick, R. L., Alptekin, G. O., Herring, A. M., Ohno, T. R., and Dec, S. F., *J. Catal.* **172**, 190 (1997).
24. Ai, M., Muneyama, E., Kunishige, A., and Ohdan, K., *J. Catal.* **144**, 632 (1993).
25. Ijjaali, M., Venturini, R., Gerardin, B., Malaman, B., and Gleitzer, C., *Eur. J. Solid State Inorg. Chem.* **28**, 983 (1991).
26. Bonnet, P., Millet, J. M. M., Leclercq, C., and Vedrine, J. C., *J. Catal.* **158**, 128 (1996).
27. Annapragada, A., and Gulari, E., *J. Catal.* **123**, 130 (1990).
28. Wandelt, K., *Surf. Sci. Rep.* **2**, 1 (1982).
29. Hawn, D. D., and DeKoven, B. M., *Surf. Interface Anal.* **10**, 63 (1987).
30. Millet, J. M. M., Virely, C., Forissier, M., Bussiere, P., and Vedrine, J. C., *Hyperfine Interactions* **46**, 619 (1989).
31. De Guire, M. R., Prasanna, T. R. S., Kalonji, G., and O'Handley, R. C., *J. Am. Ceram. Soc.* **70**, 831 (1987).
32. Modaressi, A., Courtois, A., Gerardin, R., Malaman, B., and Bleitzer, C., *J. Solid State Chem.* **47**, 245 (1983).
33. Alptekin, G. O., Williamson, D., Ohno, T. R., and McCormick, R. L., in preparation.
34. Khan, M. M., and Somorjai, G. A., *J. Catal.* **91**, 263 (1985).